

LASERS: LATent Space Encoding for Representations with Sparsity for Generative Modeling

Xin Li

Rutgers, the State University of New Jersey
New Brunswick, NJ 08901-8554

xl598@scarletmail.rutgers.edu

Anand D. Sarwate

Rutgers, the State University of New Jersey
New Brunswick, NJ 08901-8554

ads221@soe.rutgers.edu

September 18, 2024

Abstract

Learning compact and meaningful latent space representations has been shown to be very useful in generative modeling tasks for visual data. One particular example is applying Vector Quantization (VQ) in variational autoencoders (VQ-VAEs, VQ-GANs, etc.), which has demonstrated state-of-the-art performance in many modern generative modeling applications. Quantizing the latent space has been justified by the assumption that the data themselves are inherently discrete in the latent space (like pixel values). In this paper, we propose an alternative representation of the latent space by relaxing the structural assumption than the VQ formulation. Specifically, we assume the latent space can be approximated by a union of subspaces model corresponding to a dictionary-based representation under a sparsity constraint. The dictionary is learned/updated during the training process. We apply this approach to look at two models: Dictionary Learning Variational Autoencoders (DL-VAEs) and DL-VAEs with Generative Adversarial Networks (DL-GANs). We show empirically that our more latent space is more expressive and has leads to better representations than the VQ approach in terms of reconstruction quality at the expense of a small computational overhead for the latent space computation. Our results thus suggest that the true benefit of the VQ approach might not be from discretization of the latent space, but rather the lossy compression of the latent space. We confirm this hypothesis by showing that our sparse representations also address the codebook collapse issue as found common in VQ-family models.

1. Introduction

Extracting meaningful latent representations has shown its impressive impact in various generative modeling applications and efficiently structuring the latent space is

thus of continuing interest in machine learning research. Autoencoder-based approaches implicitly assume that the latent distribution falls into exponential family distributions [28]. Without additional structural assumptions, variational autoencoders (VAEs) can suffer from “mode collapse,” which motivated the development of Vector Quantized Variational Autoencoders (VQ-VAEs) [41, 48]. This approach assumes (or enforces) a latent space that is well approximated by a Voronoi tessellation induced by quantization points (also called the “codebook”). This discretization of the latent space has seen many successes in generative modeling tasks [14, 42, 52], and the discrete codebook generated from the training phase can also help with transformer training [8, 14, 49].

Vector quantization structures the latent space (the aforementioned Voronoi tessellation) and which we is a compression algorithm for the embedding vectors since all that needs to be stored is the index of the codebook. However, associating every embedding vector to a single codebook vector is an overly strict structural constraint. One proffered justification for the discretization is that in many applications the data of interest is already discretized into finite-bit representations (such as RGB images), or is itself categorical (such as text). In this paper we will instead think of the problem as one of lossy compression of the embedding vectors. This opens the door to many different forms of lossy compression/approximation. Essentially, we can think of the problem as representation learning on the embedding vectors themselves by putting another encoder/decoder pair between the encoder/decoder of the original VAE.

We contend that compression is more important than discretization and explore an alternative compression strategy using sparse dictionary learning [13]. Specifically, we learn a dictionary that can represent the embedding vectors as sparse linear combinations of atoms from an underlying dictionary. This structural assumption is a more relaxed

version as compared to Vector Quantization since multiple codebook (dictionary) elements can be used to represent a single embedding vector. As our experiments show, this yields a much more expressive latent space. A secondary benefit over quantization is that the dictionary representation is more resistant to “codebook collapse,” which is a common issue in modern VQ-family model training with fixed-length codebooks [4]. Geometrically, we engineer the latent space to be structured as a *union of subspaces* [13]. In the next section, we will briefly review prior arts in VQ-family models, sparse coding and dictionary learning research, *etc.*

In summary, our major contributions are:

- Modeling the latent space structure issue as a compression problem to design the Dictionary Learning Variational Autoencoder model (DL-VAE) and the DL-VAE with Generative Adversarial Networks (DL-GAN) model.
- Designing effective training algorithms for these models to show how we can learn the latent space model with even more representation power.
- Demonstrating that our proposed approach improves the reconstruction quality using common image datasets such as MNIST [11], CIFAR10 [29], Oxford Flowers [33], and FFHQ [25], *etc.*
- Experimental validation of the approach in terms of addressing the codebook collapse issue as seen in VQ-family models.
- In the supplementary material we show how our model can be applied to downstream generative modeling tasks such as inpainting, super-resolution and generation with diffusion models, we have also included the ablation studies in the supplementary materials.

The primary objective of this paper is to open the door to a wider range of approaches for improving latent space representations, rather than achieving state-of-the-art performance. We contend that imposing structural constraints on the latent space seems to be the primary benefit of the VQ approach, rather than discretization. This suggests that many kinds of lossy compression technique could be beneficial in these applications.

2. Related Works

The idea of discretizing the latent space we study here was initially proposed in the context of variational autoencoders [28] and has shown great success in various generation tasks and produced state-of-the-art results. Moreover, sparse dictionary learning and its application in autoencoders have been of interest over the past few years.

VQ-VAE and VQ-VAE2. Variational autoencoders with a discretization bottleneck [41, 48] are models which are better at data compression and can avoid the posterior collapse issue [50] as seen in many other variational autoencoder-based models. VQ-VAE2 [41] is an extension over VQ-VAE with two layers of quantization, which yields even higher fidelity results.

DALL-E Based Models. the DALL-E [40] family models as proposed by OpenAI replace the vector quantization with Gumbel-Softmax for categorical reparametrization [23] so that the gradient can flow through the vector quantization bottleneck.

VQ-GAN. This variant on the VQ-VAE yields higher generation quality with perceptual loss and a generative adversarial network (GAN) [14]. The learned codebook used in the VQ stage has also been shown to be helpful for transformer training [8, 14, 49].

Stable Diffusion. The VQ-GAN can also be used to obtain a high-quality latent space for high-resolution image synthesis [42]. This provides an efficient extension on powerful but computationally demanding diffusion models [12, 21, 46].

Sparse Coding and Dictionary Learning. Many approaches have been proposed for the dictionary learning problem such as methods based on LASSO regression [30], Stochastic Gradient Descent [16], and k-SVD [1, 43]. Among the dictionary learning algorithms, most approaches are often implemented in a two stage fashion, with a sparse coding stage of implemented using either greedy pursuit algorithms, such as Matching Pursuits, Orthogonal Matching Pursuits (OMP) [13] and its more efficient variant Batch Orthogonal Matching Pursuits (Batch-OMP) [43], or thresholding algorithms, such as Iterative Hard Threshold (IHT) [7], Iterative Shrinkage and Thresholding Algorithm (ISTA) [10] and its variants, and a learnable formulation such as Learnable-ISTA (LISTA) [18], *etc.*

Other VAEs with Sparse Coding. Earlier attempts on applying sparse dictionary learning on VAE models involve learning the representation as the encoder output with a fixed dictionary based on Discrete Cosine Transform (DCT) [44], which does not yield a dictionary embedded with the rich semantic information for other potential applications, the model introduced in [44] also focuses on audio signal processing and not image data. Another more recent method proposed in [51], while taking a similar format as our model by taking the encoder output directly as the sparse codes through a dictionary learning bottleneck, however it still relies on a predetermined orthogonal dictionary and does not discuss its applicability with the discriminator network for sharper outputs. The Sparse-VAE [32], though similarly enforcing a sparsity constraint, but rather it focuses on a totally different problem where the goal is to reduce the latent space feature dimension using sparsity,

and does not learn a semantically rich dictionary.

3. Dictionary Learning of Latent Spaces

To set up a generic framework to structure the latent space, as with standard VAEs, we can structure the autoencoder class models with an encoder, a decoder, and a compression bottleneck as in Figure 1 follows [28],

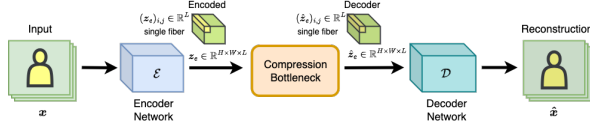


Figure 1. Architecture of a generic autoencoder model with the compression bottleneck.

Note that for the most basic VAE model, the compression bottleneck as specified in the diagram above is essentially the identity in theory, and thus $z_e = \hat{z}_e$, although in practice it often involves a reparameterization procedure for latent space sampling [28].

3.1. Prior work: Vector Quantization

An earlier successful attempt in structuring the latent space following this generic framework is to use the Vector Quantization [9], yielding the model of Vector-Quantized Variational Autoencoders (VQ-VAE) [41, 48], where we assume a discrete latent space on top of the traditional Variational Autoencoder (VAE) models [28]. The overall architecture is the same as in Figure 1, the a codebook matrix $\mathbf{E} \in \mathbb{R}^{K \times L}$ inside the compression bottleneck. Specifically, as with standard VAEs, given the input data \mathbf{x} and the latent space representation \mathbf{z} , we define the basic building blocks of the VQ-VAE model as follows,

- An encoder network \mathcal{E} which compresses the input \mathbf{x} into the latent representation \mathbf{z} by learning the parameters of a posterior distribution $q(\mathbf{z}|\mathbf{x})$;
- A prior distribution of the latent representation $p(\mathbf{z})$;
- A decoder network \mathcal{D} that can recover \mathbf{x} from the latent representation \mathbf{z} .

Then we denote the latent representation tensor generated from the encoder network \mathcal{E} as $\mathbf{z}_e \in \mathbb{R}^{H \times W \times L}$, where H and W represent the height and width dimensions of the latent space tensor, L represents the feature dimension of the latent space. Here we assume in VQ-VAE both the prior and posterior distributions are categorical. In particular, we define the set of codebook vectors $\mathcal{E} = \{e_k \in \mathbb{R}^L | k \in [K]\}$, where K is the number of embedding vectors, $[B]$ represents the set of natural numbers upper bounded by an integer $B \in \mathbb{N}^\dagger$, i.e., $[B] = \{1, 2, \dots, B\}$. We then denote the latent representation $\mathbf{z} \in \mathbb{R}^{H \times W}$ computed by

the nearest-neighbor index mapping between the latent feature vectors and the shared codebook/embedding matrix $\mathbf{E} \in \mathbb{R}^{K \times L}$, formed by stacking the codebook vectors from the set \mathcal{E} , where each entry of \mathbf{z} represents the index of the corresponding embedding vector in the codebook. The derived categorical distribution for (i, j) -th fiber where $i \in [H], j \in [W]$ is as the following,

$$q(z_{ij} = k|\mathbf{x}) = \begin{cases} 1 & \text{if } k = \arg \min_{k'} \|(z_e)_{ij} - e_{k'}\|_2; \\ 0 & \text{otherwise.} \end{cases} \quad (1)$$

Finally, we denote the quantized latent representation tensor as $\hat{\mathbf{z}}_e \in \mathbb{R}^{H \times W \times L}$, constructed by stacking the embedding vectors as indexed by the latent code \mathbf{z} ,

$$(\hat{\mathbf{z}}_e)_{ij} = e_k \text{ where } z_{ij} = k. \quad (2)$$

The quantized latents are then passed in to the decoder network \mathcal{D} that learns the distribution $p(\mathbf{x}|\hat{\mathbf{z}}_e)$ to generate the reconstruction. The training objective of the VQ-VAE model can be expressed as a modified version of the ELBO loss [14, 24, 48],

$$\ell_{\text{VQ-VAE}}(\mathbf{x}, \hat{\mathbf{x}}) = \ell_{\text{recon}}(\mathbf{x}, \hat{\mathbf{x}}) + \|\text{sg}[\mathbf{z}_e] - \hat{\mathbf{z}}_e\|_2^2 + \beta \|\mathbf{z}_e - \text{sg}[\hat{\mathbf{z}}_e]\|_2^2, \quad (3)$$

where,

$$\hat{\mathbf{z}}_e = \text{one-hot}[\mathbf{z}] \cdot \mathbf{E} \in \mathbb{R}^{H \times W \times L}. \quad (4)$$

The `one-hot` operator above performs one-hot encoding on the latent code $\mathbf{z} \in \mathbb{R}^{H \times W}$ and converts it into an $H \times W \times L$ tensor, where each fiber along the channel dimension,

$$(\text{one-hot}[\mathbf{z}])_{ij} = \mathbb{1}_{\mathbf{z}}(k) = \begin{cases} 1 & k = z, \\ 0 & \text{otherwise.} \end{cases} \in \mathbb{R}^K. \quad (5)$$

The `sg[·]` operator in Equation (3) denotes the stop gradient operation, which essentially detaches the operand tensor from the computation graph as in most modern deep learning frameworks based on automatic differentiation engines [38]. The ℓ_{recon} in Equation 13 is a generic loss function to measure reconstruction quality, where in our experiments we use a combination of the ℓ_2 loss and the perceptual loss $\ell_{\text{perceptual}}$ [53] as suggested in [14] for better results in perceptual quality,

$$\mathcal{L}_{\text{recon}}(\mathbf{x}, \hat{\mathbf{x}}) = \eta \|\mathbf{x}, \hat{\mathbf{x}}\|_2^2 + (1 - \eta) \cdot \ell_{\text{perceptual}}(\mathbf{x}, \hat{\mathbf{x}}), \quad (6)$$

with η being a weighting factor that determines the ratio of ℓ_2 loss and perceptual loss in the overall reconstruction loss function, in practice we find out that setting $\eta = 0.5$ yields satisfying results. The second and third term in Equation (3) optimize the encoder output and the codebook alternatively

by fixing either one term in the ℓ_2 loss, the β term associated with the third loss term in Equation (3) is called the *commitment loss* [48], which is used to constrain the third term so that it does not grow too large for the overall objective function to converge. A hard coded value of 0.25 for β has been shown to be effective in our experiments in align with [48].

Note also that the Vector Quantization procedure involves a nearest-neighbor mapping which is not differentiable. In practice we apply a straight-through gradient estimator [6] to copy the gradients from the encoder output directly to the compression bottleneck output:

$$\hat{z}_e = z_e + \text{sg}[\hat{z}_e - z_e]. \quad (7)$$

As with standard VAEs, the quantization/discretization process happens in between the encoder and the decoder can also be thought of as the compression bottleneck of the model, which is crucial to the model performance in terms of data representation.

Note that this formulation of the latent space can also be modeled into a probability distribution, which makes it viable to be thought of as a VAE [28]. Specifically, the sparsity of the coefficients for combining the dictionary atoms is modeled with a Mixture-of-Gaussian distribution [34] where one Gaussian captures nonactive coefficients with a small-variance distribution centered at zero, and one or more other Gaussian capture active coefficients with a large-variance distribution. More concretely, for the latent representation problem $z_e = \gamma D$, $\text{supp}\{\gamma\} = S$, the prior probability distribution over the coefficients γ_k , $k = 1, 2, \dots, K$, is factorial, with the distribution over each coefficient γ_k modeled as a Mixture-of-Gaussians distribution with two Gaussians. Then we have a set of binary state variables $a_k \in \{0, 1\}$ to determine which Gaussian is used to describe the coefficients.

The total prior over both sets of variables γ and \mathbf{a} , is of the form,

$$q(\gamma, \mathbf{a}) = \prod_{k=1}^K q(\gamma_k | a_k) q(a_k), \quad (8)$$

where $q(a_i)$ determines the probability of being in the active or inactive states, and $q(\gamma_k | s_k)$ is a Gaussian distribution whose mean and variance is determined by the current state s_k .

The total probability for the latent representation can then be modeled by,

$$q(z_e; \theta) = \sum_{\mathbf{a}} q(\mathbf{s}; \theta) \int q(z_e | \gamma, \theta) q(\gamma | \mathbf{a}; \theta) d\gamma. \quad (9)$$

3.2. Structuring with Dictionary Learning

Vector Quantization compresses the latent space into a discrete set of codebook vectors. Our proposal is to use a

different form of lossy compression by putting representation learning inside the VAE (essentially learning a better representation of the latent representations). Specifically, we apply sparse dictionary learning [13] that allows for richer representations/structuring of the embedding space than the vector quantization. In dictionary-based representations, each embedding vector is approximated by a sparse linear combination of embedding vectors (dictionary atoms). This allows multiple atoms to represent one embedding vector and allows the contribution of each atom to vary its level of contribution by its coefficient. We show in our experimental work that this approach gives much stronger representing power with a modest computational overhead.

Specifically, given the set of dictionary atoms $\mathcal{D} = \{\mathbf{d}_k \in \mathbb{R}^L | k = 1, 2, \dots, K\}$, we consider a sparse set of dictionary atoms whose the linear combination represents that individual latent feature vector, where we define number of dictionary atoms used for each latent feature vector as the sparsity level as $S \in \mathbb{N}^+$ (note that when $S = 1$, we essentially get the VQ-VAE). Then we have the latent representation becomes a tensor $\mathbf{z} \in \mathbb{R}^{H \times W \times S}$, where each vector $\mathbf{z}_{ij} \in \mathbb{R}^S$ represents an indexing vector to select a sparse set of S dictionary atoms. The compressed latent representation \mathbf{z} directly corresponds to the sparse representation coefficient matrix, also known as the sparse codes, denoted as $\gamma \in \mathbb{R}^{H \times W \times K}$, with each single fiber $\gamma_{ij} \in \mathbb{R}^K$, $i \in [H]$, $j \in [W]$,

$$\gamma_{ij}, \mathbf{D} = \arg \min_{\tilde{\gamma}_{ij}, \tilde{\mathbf{D}}} \|(z_e)_{ij} - \tilde{\gamma}_{ij} \tilde{\mathbf{D}}\|_2, \quad (10)$$

$$\text{subject to } \text{supp}\{\gamma_{ij}\} = S, \quad (11)$$

where the $\mathbf{D} \in \mathbb{R}^{K \times L}$ is the dictionary matrix constructed from stacking the dictionary atom vectors in the dictionary set \mathcal{D} , $\text{supp}(\gamma_{ij})$ denotes the support of the sparse code vector γ_{ij} , which is defined the ℓ_0 norm of the vector, *i.e.*, $\text{supp}(\gamma_{ij}) = \|\gamma_{ij}\|_0$. We name the derived model as Dictionary Learning Variational Autoencoder (DL-VAE). The high-level working mechanism of the DL-VAE model still follows the generic framework as depicted in Figure 1, with the compression bottleneck block containing a dictionary matrix $\mathbf{D} \in \mathbb{R}^{K \times L}$.

Note that in conventional dictionary learning setting we expect to solve an overcomplete problem [13], where we assume the feature dimension L should be no greater than the number of dictionary atoms K . Furthermore, as the input image resolution gets higher, a larger latent space is required to maintain the representation quality, making it challenging to model the latent space distribution for the whole image. Thus in practice, we typically adopt a patch-level coding [35–37], where we first unfold the latent space

representation as non-overlapping patches¹ of dimension $P_H \times P_W \times L$ such that $P_H \times P_W \leq K$ before we perform the dictionary learning procedure to reconstruct the patches, where P_H, P_W represents the respective height and width dimension of the patches or unfolding kernel size in implementation, then we reconstruct the latent space representation by folding back the reconstructed patches. The model shares the same versatility of choices of encoder and decoder architectures as the VQ family models (VQ-VAE, VQ-GAN, *etc.*) [14, 41, 48]. As for the compression bottleneck based on dictionary learning, we first assume the dictionary is prefixed and perform a sparse coding stage [10, 18, 43, 47], and then learn the dictionary via common momentum-based stochastic gradient optimizers [20, 27] while fixing the learned sparse codes. The diagram of the internal mechanism of the dictionary learning compression bottleneck is shown in Figure 3 (a).

3.3. Selecting the Best Dictionary Atoms

To select the best sparse set of dictionary atoms and coefficients for the linear combinations, we first assume the learned dictionary is fixed, then perform the sparse coding procedure in the dictionary learning bottleneck on the encoded input. While there exist many methods for sparse coding, we adopted Batch Orthogonal Matching Pursuit (Batch-OMP) [43] to compute the sparse codes for dictionary atom combination, a greedy approach that selects the best matching dictionary atoms with target sparsity and precision, which has demonstrated better convergence property than thresholding based methods [13] and is easier to be separated from the dictionary training as compared to other learnable procedures such as LISTA [18]. Specifically, we keep selecting the dictionary atoms with maximum correlation to the input signals and then perform a progressive Cholesky procedure [43] to solve for the sparse codes.

After the sparse coding procedure, we compute the latent space reconstruction \hat{z}_e by multiplying the sparse codes and the dictionary matrix,

$$(\hat{z}_e)_{ij} = \gamma_{ij} \mathbf{D}, \quad i \in [H], j \in [W]. \quad (12)$$

Then pass it through the decoder to get the reconstruction \hat{x} , the quality of the reconstruction is then measured by common image reconstruction metrics such as the MSE, PSNR, SSIM and deep learning based metrics such as LPIPS [53] and the FLIP metric [2], *etc.*

Note that during training, given an input tensor \mathbf{x} , both the sparse codes and the dictionary loss are jointly opti-

¹While conventionally people use overlapping image patches to make sure patches are related to each other, in our scenario since we already have a convolutional encoder and decoder network that make sure each latent feature vector covers an overlapping region of the original image, thus we do not need to create overlapping patches in the latent space, saving some additional compute time.

mized as in the VQ-VAE model, with the combined objective for input \hat{x} ,

$$\begin{aligned} \ell_{\text{DL-VAE}}(\mathbf{x}, \hat{\mathbf{x}}) &= \ell_{\text{recon}}(\mathbf{x}, \hat{\mathbf{x}}) + \|\text{sg}[z_e] - \hat{z}_e\|_2^2 + \\ &\quad \beta \|z_e - \text{sg}[\hat{z}_e]\|_2^2, \\ \hat{z}_e &= \gamma \cdot \mathbf{D} \in \mathbb{R}^{H \times W \times L}. \end{aligned} \quad (13)$$

Note that here the sparse codes γ are calculated via the sparse coding procedure described above, which involves a non-differentiable argmax operation, thus following the similar idea adopted in VQ-VAE training, we apply a straight-through gradient estimator to make sure the gradient backpropagates through the entire computational graph approximately. By incorporating the dictionary-related loss term (Equation 13) in the objective, the model will perform an implicit online dictionary update [30, 39] with modern momentum-based stochastic optimization methods [20, 27]. Geometrically speaking, the dictionary atoms in combination with the precomputed sparse codes will move towards the latent feature vectors from the encoder output (as shown in Figure 3 (a)). Note that here we can also use a learning rate free rule to update the dictionary in an online manner as proposed by [30], but in practice it proves to be slow as the number of dictionary atoms increase and does not yield a superior performance. Also here we do not use the traditional dictionary learning algorithms as the datasets we use are rather large and thus not fit for traditional dictionary learning algorithms where we expect to use the entire dataset [1, 13, 43].

3.4. Deblurring with the Discriminator Network

Following the same idea as in [14], the DL-VAE model can also be enhanced by appending a discriminator network, *i.e.*, the PatchGAN [22] to produce even sharper output. Specifically, we introduce a patch-based discriminator \mathcal{D} that will try to distinguish the original image (\mathbf{x}) and the reconstructed image ($\hat{\mathbf{x}}$) using the GAN objective,

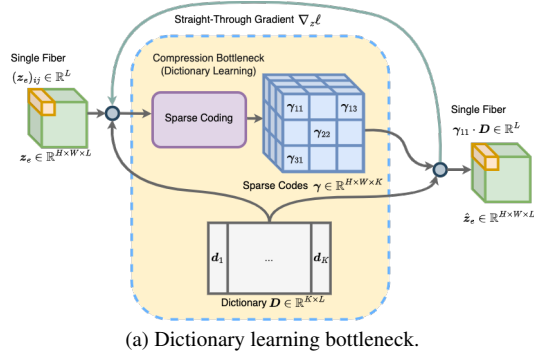
$$\ell_{\text{GAN}}(\{\mathcal{E}, \mathcal{G}, \mathcal{Z}\}, \mathcal{D}) = [\log \mathcal{D}(\mathbf{x}) + \log(1 - \mathcal{D}(\hat{\mathbf{x}}))], \quad (14)$$

where \mathcal{G} denotes the generic generative network, which is just the decoder network \mathcal{D} in our VAE models. The we have the complete objective for the DL-GAN model $\Omega^* = \{\mathcal{E}^*, \mathcal{G}^*, \mathcal{Z}^*\}$ is the solution to the minimax game,

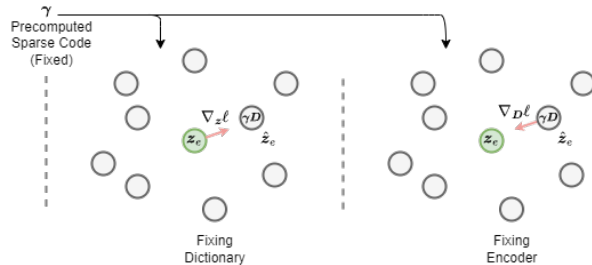
$$\begin{aligned} \Omega^* &= \arg \min_{\mathcal{E}, \mathcal{G}, \mathcal{Z}} \max_{\mathcal{D}} \mathbb{E}_{p_{\mathcal{D}}(\mathbf{x})} [\ell_{\text{DL-VAE}}(\mathcal{E}, \mathcal{G}, \mathcal{Z}) + \\ &\quad \lambda \ell_{\text{GAN}}(\{\mathcal{E}, \mathcal{G}, \mathcal{Z}\}, \mathcal{D})], \end{aligned} \quad (15)$$

where the λ is the adaptive weight computed as follows,

$$\lambda = \frac{\nabla_{\mathcal{G}_\ell} [\ell_{\text{recon}}]}{\nabla_{\mathcal{G}_\ell} [\ell_{\text{GAN}}] + \delta} \quad (16)$$



(a) Dictionary learning bottleneck.



(b) Dictionary atoms and encoder outputs during training.

Figure 2. (a) The internal working mechanism of the Dictionary Learning Compression Bottleneck. Note that here each fiber of the latent sparse codes is of K length, however, due to the sparse structure assumption, we can always represent the sparse codes in a sparse data structure, such as the Sparse COO, CSR, *etc.*, data formats [13, 38], in which the fibers can be reduced to $S \ll K$ length; (b) How the encoder outputs and the dictionary atoms move towards each other during training.

where $\nabla_{\Theta_L} [\cdot]$ denotes the corresponding gradient with respect to the last layer of the decoder, and δ is small constant for numerical stability, where we pick $\delta = 10^{-6}$ in our experiments. The overall architecture for the DL-GAN model is shown in Figure 3 below,

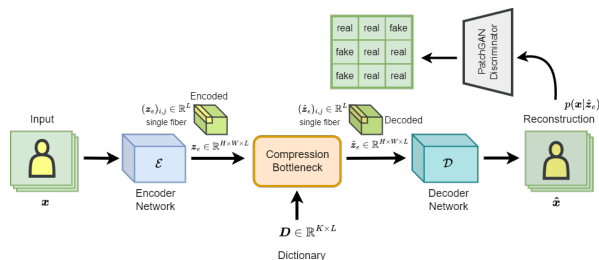


Figure 3. High-level architectural overview of DL-GAN.

4. Evaluation Methods

Here to evaluate the reconstruction quality for the images, we adopt the conventional image evaluation metric Peak Signal-to-Noise Ratio (PSNR) [15] and the deep learning based metrics LPIPS [53] loss and the FLIP loss [2], which tends to focus more on perceptual quality instead of pixel by pixel recovery by comparing the image features extracted by deep neural networks instead of the image pixels directly. To evaluate the model’s performance on addressing codebook collapse issue as introduced by VQ-family models, we compute the perplexity to measure the usage of either codebook or dictionary atom usage [9], which is defined as the exponent of average log likelihood of all embedding vectors in an input sequence,

$$\text{ppl}(\mathbf{W}) = \exp \left\{ -\frac{1}{N} \sum_{i=1}^N \log p(\mathbf{w}_i | \mathbf{w}_{<i}) \right\}, \quad (17)$$

where $\text{ppl}(\mathbf{W})$ denotes the perplexity of codebook matrix \mathbf{W} containing N codewords $\mathbf{w}_i, i = 1, 2, \dots, N$. We use UMAP [31] to visualize the vectors.

5. Experiments

In our experiments, we adopt a similar lightweight encoder-decoder architecture for our model as proposed in [48], with the encoder network consists of 2 strided convolutional layers with stride 2 and kernel size 4×4 , followed by two residual blocks of size 3×3 (implemented as ReLU + 3×3 convolutional layer + 1×1 convolutional layer), all having 128 hidden units. Similarly for the decoder network we have two 3×3 residual blocks, followed by two transposed convolutions with stride 2 and kernel size 4×4 . We use the Adam optimizer [27] with a learning rate of 1×10^{-4} for both VQ-family models and the DL-family models training. We also implement both the codebook in the VQ-family models and the dictionary in the DL-family models as an embedding layer, with dimension of 512×16 , containing 512 latent embedding vectors of feature dimension 16. For the VQ-family model training, we adopt a procedure based on the Exponential Moving Average (EMA) with a decay rate of 0.99, which proves to converge faster and handle codebook collapse better [3, 4, 48]. As for the DL-family model training, we use a sparsity level of 5, which allows 5 dictionary atoms to be used in the linear combination to represent each latent feature vector.

For the training experiments, we tested the model VQ-VAE and DL-VAE with the Oxford Flowers [33] dataset, which contains over 1,000 high quality flower images, we augment the dataset by extracting random crops of 256×256 images and train both models for 1,000 epochs, the results of the training experiments are shown in Figure 4.

From the training experiments we can see that the DL-VAE converges at a much higher reconstruction PSNR as

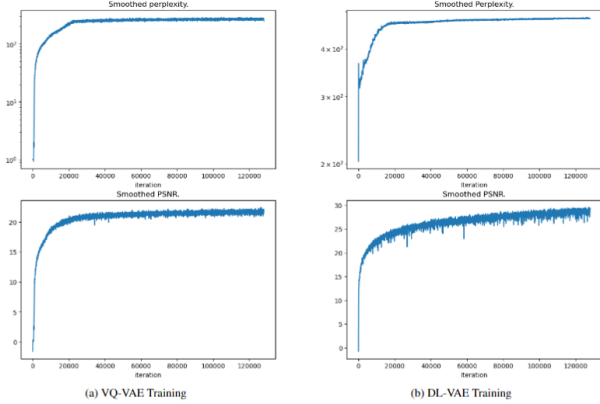


Figure 4. (a) The training evolution of the VQ-VAE model; Figure (b) The training evolution of the DL-VAE model. For both models we evaluate the codebook/dictionary perplexity and the reconstruction PSNR, both in a smoothed fashion using the Savitzky–Golay filter [45].

compared to the VQ-VAE, also the DL-VAE does not suffer codebook collapse, reaching a much higher perplexity value. In particular, the VQ-VAE has a perplexity of 275 with a PSNR of 21.9 whereas our DL-VAE has a perplexity of 507 with a PSNR of 29.1.

5.1. Latent Space Reconstructions

Since both models essentially perform latent space reconstruction with different forms of lossy compression, we can evaluate the latent space reconstruction quality from the two compression bottlenecks, here we take results from earlier stages of training (10 epochs) so that we can spot on the difference between the two compression bottlenecks on the latent space more easily (when both models converge the differences are not easily visible). Since the latent feature dimension is 16 which is too high for a sensible visualization, we extract the top singular components from the latent spaces and project them on the grayscale space,

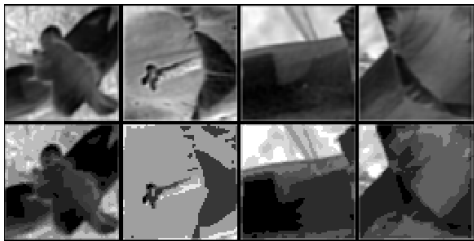


Figure 5. Figures on the first row shows the top singular component from the VQ-VAE encoder output; Figures on the bottom row shows the top singular component from the early stage latent space reconstruction via the Vector Quantization bottleneck.

Note that here from Figure 5 we can clearly see the effect of vector quantization at the early stage of training, with a

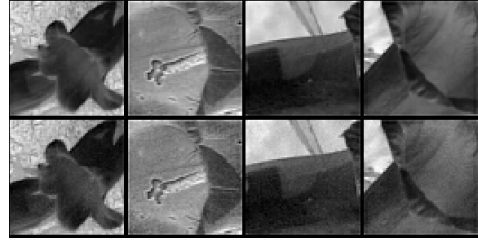


Figure 6. Figures on the first row shows the top singular component from the VQ-VAE encoder output; Figures on the bottom row shows the top singular component from the early stage latent space reconstruction via the Vector Quantization bottleneck.

lot of quantization artifacts in the latent space, however as we can see the reconstructions from the dictionary learning bottleneck are a lot smoother, aligning with our intuition of a more relaxed structural constraint. More concretely, we calculated the reconstruction MSE loss for both models, with the loss of the VQ-VAE model being 0.0701 and 0.0039 for the DL-VAE model.

5.2. The Embedding Visualizations

To further validate the DL bottleneck’s ability in circumventing codebook collapse, we reshape the 16 dimensional embedding vectors into 4 patches and visualize them in grayscale images, we have also provided a visualization of the embedding vector distribution in the latent space using UMAP [31]. The visualizations regarding the VQ-VAE and the DL-VAE models are shown in Figure 7 and Figure 8 respectively.



Figure 7. (a) grayscale images of the reshaped codebook vectors. (b) Codebook vector distribution in the embedding space.

From the visualizations, we can clearly see the codebook collapse phenomenon in the VQ-VAE model, where all the codebook vectors tend to cluster to each other and are rather similar in the look, while the dictionary atoms are distributed in a more spread out fashion with much different looks from each other.

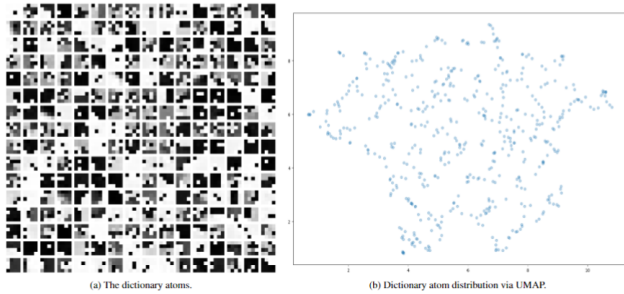


Figure 8. (a) grayscale images of the reshaped dictionary atoms. (b) Dictionary atom distribution in the embedding space.

5.3. The Reconstructions

Here are the reconstructions from our trained models on Oxford Flowers dataset [33], to highlight the differences between the reconstructions and the original images, we apply the FLIP heatmap to both model outputs, where the darker the region in the heatmap, the more fidelity in reconstruction, and the discrepancies in the reconstructions are thus visualized in highlighted regions.

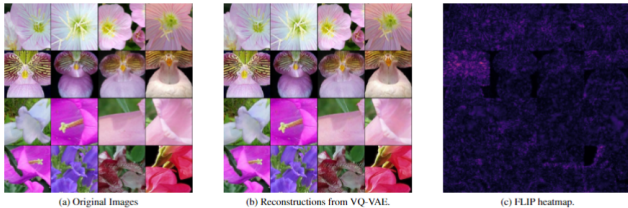


Figure 9. (a) Original Images. (b) Reconstructions from VQ-VAE. (c) FLIP heatmap.

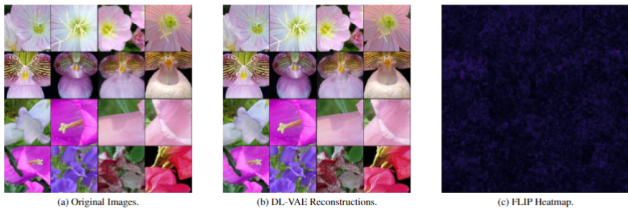


Figure 10. (a) Original Images. (b) Reconstructions from DL-VAE. (c) FLIP heatmap.

Some further reconstructions results on the FFHQ dataset [25], along with the VQ-GAN and the proposed DL-GAN models are shown in the Figure 11 and the Figure 12,

Here is the table summarizing the model reconstruction PSNR on various datasets,

6. Conclusion and Future Work

In this paper, we examined the effectiveness of latent space representation learning by sparse dictionary learning



Figure 11. Reconstruction visualizations of VQ-GAN, DL-VAE, and DL-GAN with sparsity level 5, the first row are original images from the FFHQ dataset, while the second row are the VQ-GAN reconstructions, the third row are the DL-VAE reconstructions, and the fourth row are the DL-GAN reconstructions.



Figure 12. FLIP heatmap visualizations of VQ-GAN, DL-VAE, and DL-GAN with sparsity level 5, the images in the first row are the FLIP heatmap between the original images and the VQ-GAN reconstructions, the images in the second row are the FLIP heatmap between the original images and the DL-VAE reconstructions, the images in the third row are the FLIP heatmap between the original images and the DL-GAN reconstructions.

Model	MNIST	CIFAR10	Oxford Flowers	FFHQ
VQ-VAE	18.1	22.9	21.9	23.8
VQ-GAN	19.3	23.2	22.5	24.6
DL-VAE	25.9	29.2	29.1	32.2
DL-GAN	27.2	31.1	31.4	33.7

Table 1. Reconstruction PSNRs attained from training on various datasets. All PSNR values are reported upon training convergence.

instead of the vector quantization, and demonstrated that the effectiveness of vector quantization in previous mod-

els might not be the only answer to effective latent representation learning. The derived models, DL-VAE and DL-GAN have demonstrated solid performance in terms of latent space representation power and robustness to codebook collapse. Also be aware that the sparsity assumption we are using, though demonstrating strong performance against the VQ-family models, still is not the only best way to represent the latent space, this idea leaves huge room for further research in terms of the representation learning in latent space and using this learned representation to support other state-of-the-art generative models [8, 14, 42], etc.

References

- [1] M. Aharon, M. Elad, and A. Bruckstein. K-svd: An algorithm for designing overcomplete dictionaries for sparse representation. *IEEE Transactions on Signal Processing*, 54(11):4311–4322, 11 2006. [2](#), [5](#)
- [2] Pontus Andersson, Jim Nilsson, Tomas Akenine-Möller, Magnus Oskarsson, Kalle Åström, and Mark D. Fairchild. Flip: A difference evaluator for alternating images. *Proc. ACM Comput. Graph. Interact. Tech.*, 3(2), 8 2020. [5](#), [6](#)
- [3] Anonymous. Exponential moving average of weights in deep learning: Dynamics and benefits. *Submitted to Transactions on Machine Learning Research*, 2023. Under review. [6](#)
- [4] Gulcin Baykal, Melih Kandemir, and Gozde Unal. Edvae: Mitigating codebook collapse with evidential discrete variational autoencoders. *Pattern Recognition*, 156:110792, 2024. [2](#), [6](#)
- [5] Amir Beck and Marc Teboulle. A fast iterative shrinkage-thresholding algorithm with application to wavelet-based image deblurring. In *2009 IEEE International Conference on Acoustics, Speech and Signal Processing*, pages 693–696, April 2009. [12](#)
- [6] Yoshua Bengio, Nicholas Léonard, and Aaron Courville. Estimating or propagating gradients through stochastic neurons for conditional computation. *arXiv preprint arXiv:1308.3432*, 2013. [4](#)
- [7] Thomas Blumensath and Mike E Davies. Iterative hard thresholding for compressed sensing. *Applied and computational harmonic analysis*, 27(3):265–274, 2009. [2](#)
- [8] Tom Brown, Benjamin Mann, Nick Ryder, Melanie Subbiah, Jared D Kaplan, Prafulla Dhariwal, Arvind Neelakantan, Pranav Shyam, Girish Sastry, Amanda Askell, et al. Language models are few-shot learners. *Advances in neural information processing systems*, 33:1877–1901, 2020. [1](#), [2](#), [9](#)
- [9] T.M. Cover and J.A. Thomas. *Elements of Information Theory*. Wiley, New York, 1991. [3](#), [6](#)
- [10] Ingrid Daubechies, Michel Defrise, and Christine De Mol. An iterative thresholding algorithm for linear inverse problems with a sparsity constraint. *Communications on Pure and Applied Mathematics: A Journal Issued by the Courant Institute of Mathematical Sciences*, 57(11):1413–1457, 2004. [2](#), [5](#), [12](#)
- [11] Li Deng. The mnist database of handwritten digit images for machine learning research. *IEEE Signal Processing Magazine*, 29(6):141–142, 2012. [2](#)
- [12] Prafulla Dhariwal and Alexander Nichol. Diffusion models beat gans on image synthesis. *Advances in neural information processing systems*, 34:8780–8794, 2021. [2](#)
- [13] Yonina C. Eldar and Gitta Kutyniok. *Compressed Sensing: Theory and Applications*. Cambridge University Press, 2012. [1](#), [2](#), [4](#), [5](#), [6](#), [12](#), [13](#)
- [14] Patrick Esser, Robin Rombach, and Bjorn Ommer. Taming transformers for high-resolution image synthesis. In *Proceedings of the IEEE/CVF conference on computer vision and pattern recognition*, pages 12873–12883, 2021. [1](#), [2](#), [3](#), [5](#), [9](#), [13](#)
- [15] Fernando A Fardo, Victor H Conforto, Francisco C de Oliveira, and Paulo S Rodrigues. A formal evaluation of psnr as quality measurement parameter for image segmentation algorithms. *arXiv preprint arXiv:1605.07116*, 2016. [6](#)
- [16] Dar Gilboa, Sam Buchanan, and John Wright. Efficient dictionary learning with gradient descent. In *International Conference on Machine Learning*, pages 2252–2259. PMLR, 2019. [2](#)
- [17] G.H. Golub and C.F. Van Loan. *Matrix Computations*. Johns Hopkins Studies in the Mathematical Sciences. Johns Hopkins University Press, 2013. [12](#)
- [18] Karol Gregor and Yann LeCun. Learning fast approximations of sparse coding. In *Proceedings of the 27th international conference on international conference on machine learning*, pages 399–406, 2010. [2](#), [5](#), [12](#)
- [19] Martin Heusel, Hubert Ramsauer, Thomas Unterthiner, Bernhard Nessler, and Sepp Hochreiter. Gans trained by a two time-scale update rule converge to a local nash equilibrium. *Advances in neural information processing systems*, 30, 2017. [16](#)
- [20] Geoffrey Hinton, Nitish Srivastava, and Kevin Swersky. Neural networks for machine learning lecture 6a overview of mini-batch gradient descent. *Cited on*, 14(8):2, 2012. [5](#)
- [21] Jonathan Ho, Ajay Jain, and Pieter Abbeel. Denoising diffusion probabilistic models. *Advances in neural information processing systems*, 33:6840–6851, 2020. [2](#), [18](#)
- [22] Phillip Isola, Jun-Yan Zhu, Tinghui Zhou, and Alexei A Efros. Image-to-image translation with conditional adversarial networks. In *Proceedings of the IEEE conference on computer vision and pattern recognition*, pages 1125–1134, 2017. [5](#), [13](#)
- [23] Eric Jang, Shixiang Gu, and Ben Poole. Categorical reparameterization with gumbel-softmax. *arXiv preprint arXiv:1611.01144*, 2016. [2](#)
- [24] Michael I Jordan, Zoubin Ghahramani, Tommi S Jaakkola, and Lawrence K Saul. An introduction to variational methods for graphical models. *Machine learning*, 37:183–233, 1999. [3](#)
- [25] Tero Karras, Samuli Laine, and Timo Aila. A style-based generator architecture for generative adversarial networks. In *Proceedings of the IEEE/CVF conference on computer vision and pattern recognition*, pages 4401–4410, 2019. [2](#), [8](#), [13](#)
- [26] R. Keys. Cubic convolution interpolation for digital image processing. *IEEE Transactions on Acoustics, Speech, and Signal Processing*, 29(6):1153–1160, 1981. [16](#)
- [27] Diederik P Kingma. Adam: A method for stochastic optimization. *arXiv preprint arXiv:1412.6980*, 2014. [5](#), [6](#)
- [28] Diederik P Kingma and Max Welling. Auto-encoding variational bayes. *arXiv preprint arXiv:1312.6114*, 2013. [1](#), [2](#), [3](#), [4](#)
- [29] Alex Krizhevsky, Geoffrey Hinton, et al. Learning multiple layers of features from tiny images. Technical report, University of Toronto, 2009. [2](#), [13](#), [14](#), [15](#)
- [30] Julien Mairal, Francis Bach, Jean Ponce, and Guillermo Sapiro. Online dictionary learning for sparse coding. In *Proceedings of the 26th annual international conference on machine learning*, pages 689–696, 2009. [2](#), [5](#), [12](#), [13](#)

- [31] Leland McInnes, John Healy, and James Melville. Umap: Uniform manifold approximation and projection for dimension reduction. *arXiv preprint arXiv:1802.03426*, 2018. [6](#), [7](#)
- [32] Gemma E Moran, Dhanya Sridhar, Yixin Wang, and David M Blei. Identifiable deep generative models via sparse decoding. *arXiv preprint arXiv:2110.10804*, 2021. [2](#)
- [33] Maria-Elena Nilsback and Andrew Zisserman. Automated flower classification over a large number of classes. In *Indian Conference on Computer Vision, Graphics and Image Processing*, Dec 2008. [2](#), [6](#), [8](#), [16](#)
- [34] Bruno Olshausen and K. Millman. Learning sparse codes with a mixture-of-gaussians prior. In S. Solla, T. Leen, and K. Müller, editors, *Advances in Neural Information Processing Systems*, volume 12. MIT Press, 1999. [4](#)
- [35] Bruno A Olshausen and David J Field. Emergence of simple-cell receptive field properties by learning a sparse code for natural images. *Nature*, 381(6583):607–609, 1996. [4](#)
- [36] Bruno A. Olshausen and David J. Field. Sparse coding with an overcomplete basis set: A strategy employed by v1? *Vision Research*, 37(23):3311–3325, 1997. [4](#)
- [37] Bruno A Olshausen and David J Field. Sparse coding of sensory inputs. *Current Opinion in Neurobiology*, 14(4):481–487, 2004. [4](#)
- [38] Adam Paszke, Sam Gross, Francisco Massa, Adam Lerer, James Bradbury, Gregory Chanan, Trevor Killeen, Zeming Lin, Natalia Gimelshein, Luca Antiga, Alban Desmaison, Andreas Kopf, Edward Yang, Zachary DeVito, Martin Raison, Alykhan Tejani, Sasank Chilamkurthy, Benoit Steiner, Lu Fang, Junjie Bai, and Soumith Chintala. Pytorch: An imperative style, high-performance deep learning library. In *Advances in Neural Information Processing Systems 32*, pages 8024–8035. Curran Associates, Inc., 2019. [3](#), [6](#)
- [39] Sirisha Rambhatla, Xingguo Li, and Jarvis Haupt. Noodl: Provable online dictionary learning and sparse coding. *arXiv preprint arXiv:1902.11261*, 2019. [5](#)
- [40] Aditya Ramesh, Mikhail Pavlov, Gabriel Goh, Scott Gray, Chelsea Voss, Alec Radford, Mark Chen, and Ilya Sutskever. Zero-shot text-to-image generation. In Marina Meila and Tong Zhang, editors, *Proceedings of the 38th International Conference on Machine Learning*, volume 139 of *Proceedings of Machine Learning Research*, pages 8821–8831. PMLR, 7 2021. [2](#)
- [41] Ali Razavi, Aaron van den Oord, and Oriol Vinyals. Generating diverse high-fidelity images with vq-vae-2. In H. Wallach, H. Larochelle, A. Beygelzimer, F. d'Alché-Buc, E. Fox, and R. Garnett, editors, *Advances in Neural Information Processing Systems*, volume 32. Curran Associates, Inc., 2019. [1](#), [2](#), [3](#), [5](#), [13](#)
- [42] Robin Rombach, Andreas Blattmann, Dominik Lorenz, Patrick Esser, and Björn Ommer. High-resolution image synthesis with latent diffusion models. In *Proceedings of the IEEE/CVF conference on computer vision and pattern recognition*, pages 10684–10695, 2022. [1](#), [2](#), [9](#), [15](#), [18](#)
- [43] Ron Rubinfeld, Michael Zibulevsky, and Michael Elad. Efficient implementation of the k-svd algorithm using batch orthogonal matching pursuit. *CS Technion*, 40, 01 2008. [2](#), [5](#), [12](#)
- [44] Mostafa Sadeghi and Paul Magron. A sparsity-promoting dictionary model for variational autoencoders. *arXiv preprint arXiv:2203.15758*, 2022. [2](#)
- [45] Abraham Savitzky and M. J. E. Golay. Smoothing and differentiation of data by simplified least squares procedures. *Analytical Chemistry*, 36(8):1627–1639, 1964. [7](#)
- [46] Jascha Sohl-Dickstein, Eric Weiss, Niru Maheswaranathan, and Surya Ganguli. Deep unsupervised learning using nonequilibrium thermodynamics. In *International conference on machine learning*, pages 2256–2265. PMLR, 2015. [2](#)
- [47] Joel A. Tropp and Anna C. Gilbert. Signal recovery from random measurements via orthogonal matching pursuit. *IEEE Transactions on Information Theory*, 53(12):4655–4666, Dec 2007. [5](#), [12](#)
- [48] Aaron Van Den Oord, Oriol Vinyals, et al. Neural discrete representation learning. *Advances in neural information processing systems*, 30, 2017. [1](#), [2](#), [3](#), [4](#), [5](#), [6](#)
- [49] Ashish Vaswani, Noam Shazeer, Niki Parmar, Jakob Uszkoreit, Llion Jones, Aidan N Gomez, Łukasz Kaiser, and Illia Polosukhin. Attention is all you need. *Advances in neural information processing systems*, 30, 2017. [1](#), [2](#)
- [50] Yixin Wang, David Blei, and John P Cunningham. Posterior collapse and latent variable non-identifiability. *Advances in Neural Information Processing Systems*, 34:5443–5455, 2021. [2](#)
- [51] Pan Xiao, Peijie Qiu, and Aristeidis Sotiras. Sc-vae: Sparse coding-based variational autoencoder. *arXiv preprint arXiv:2303.16666*, 2023. [2](#)
- [52] Jiahui Yu, Xin Li, Jing Yu Koh, Han Zhang, Ruoming Pang, James Qin, Alexander Ku, Yuanzhong Xu, Jason Baldridge, and Yonghui Wu. Vector-quantized image modeling with improved vqgan. *arXiv preprint arXiv:2110.04627*, 2021. [1](#), [13](#)
- [53] Richard Zhang, Phillip Isola, Alexei A Efros, Eli Shechtman, and Oliver Wang. The unreasonable effectiveness of deep features as a perceptual metric. In *Proceedings of the IEEE conference on computer vision and pattern recognition*, pages 586–595, 2018. [3](#), [5](#), [6](#)

LASERS: LAtent Space Encoding for Representations with Sparsity for Generative Modeling Supplementary Material

Xin Li

Rutgers, the State University of New Jersey
New Brunswick, NJ 08901-8554

x1598@scarletmail.rutgers.edu

Anand D. Sarwate

Rutgers, the State University of New Jersey
New Brunswick, NJ 08901-8554

ads221@soe.rutgers.edu

September 18, 2024

7. The Sparse Coding Algorithm

In our implementations¹ of the DL-family models (DL-VAE and DL-GAN), we adopt the Batch-OMP [43] procedure as our sparse coding algorithm, which has demonstrated superior performance in terms of efficiency and convergence as compared to other greedy pursuits and thresholding based methods [5, 10, 13, 18, 47]. Specifically, given the dictionary D , the support set \mathcal{T} ($|\mathcal{T}| = S$ for sparsity level S), and the residual r the classic greedy OMP algorithm usually involves the computation [13, 43],

$$\begin{aligned}\hat{\gamma}_{\mathcal{T}} &= D_{\mathcal{T}}^{\dagger} r \\ &= (D_{\mathcal{T}}^{\top} D_{\mathcal{T}})^{-1} D_{\mathcal{T}}^{\top} r,\end{aligned}$$

requiring the expensive matrix inversion of $D_{\mathcal{T}}^{\top} D_{\mathcal{T}}$. However, note that $D_{\mathcal{T}}^{\top} D_{\mathcal{T}}$ is actually a symmetric positive definite matrix and thus can be addressed more efficiently by progressive Cholesky factorization [17, 43]. Also the atom selection step at each iteration does not require knowing r or γ explicitly, but rather only $D^{\top} r$. Hence we can seek to replace the explicit computation of r and its multiplication by D^{\top} with a lower-cost computation $D^{\top} r$. To achieve that, denote $\alpha = D^{\top} r$, $\alpha^0 = D^{\top} y$ with y denoting the initial signal input, and $G = D^{\top} D$, we then have,

$$\begin{aligned}\alpha &= D^{\top} (y - D_{\mathcal{T}} D_{\mathcal{T}}^{\dagger} y) \\ &= \alpha^0 - G_{\mathcal{T}} D_{\mathcal{T}}^{\dagger} y \\ &= \alpha^0 - G_{\mathcal{T}} (D_{\mathcal{T}}^{\top} D_{\mathcal{T}})^{-1} D_{\mathcal{T}}^{\top} y.\end{aligned}\quad (18)$$

The algorithm pseudocode is shown below [43],

¹Please feel free to check our [GitHub Repository](#) for our codebase and experiments setups.

8. Online Dictionary Learning Based on Block-Coordinate Descent

Apart from the implicit dictionary learning method mentioned in the paper, we can also break the dictionary learning process into two stages, with the first stage being the sparse coding stage and the second stage being a learning rate free online dictionary update via Block-Coordinate Descent [30]. Specifically, at each training iteration, after passing the input from the encoder network, we first assume that the dictionary is fixed and perform the sparse coding stage (Algorithm 1) to compute the sparse code associated with the training sample. Then we adopt a Block-Coordinate Descent procedure to update the dictionary atoms based on the calculated sparse code. Specifically, on training iteration t , consider the sparse code $\gamma^{(t)}$ computed from the sparse coding stage and the minibatch input encodings $z_e^{(t)} \in \mathbb{R}^{B \times H \times W \times L}$ from the encoder, we first flatten the encodings into $\bar{z}_e^{(t)} \in \mathbb{R}^{L \times BHW}$ shape, denote $\xi = BHW$, we then calculate the moving average of the matrices from gradient computations,

$$A^{(t)} = \beta A^{(t-1)} + \gamma^{(t)} \left(\gamma^{(t)} \right)^{\top}, \quad (23)$$

$$B^{(t)} = \beta B^{(t-1)} + z_e^{(t)} \left(\gamma^{(t)} \right)^{\top}, \quad (24)$$

where β is an adaptive parameter for better convergence in practice [30],

$$\beta = \frac{\theta + 1 - \xi}{\theta + 1}, \quad (25)$$

where the parameter θ is computed as follows,

$$\theta = \begin{cases} t\xi, & \text{if } t < \xi, \\ \xi^2 + t - \xi, & \text{if } t \geq \xi. \end{cases} \quad (26)$$

Then we perform one iteration of the Block-Coordinate Descent algorithm on all the codebook embedding columns,

Algorithm 1: Batch Orthogonal Matching Pursuit (Batch-OMP) [13]

Input: one column of the flattened encoder output $(\tilde{z}_e)_n, n \in [N]$ where $N = H \times W$, embedding/dictionary matrix D , and sparsity level S

1 **Initialize:** $\alpha^0 = D^\top (\tilde{z}_e)_n$, initial gram matrix $G^{(0)} = D^\top D$

2 **for** $s \leftarrow 1; s \leftarrow s + 1; s \leftarrow S$ **do**

3 Calculate the following,

$$j^{(s)} \leftarrow \underset{j}{\operatorname{argmax}} |\alpha_j^{(s)}| \quad (19)$$

which essentially selects elements based on the magnitude of the elements of $\alpha^{(s)}$;

4 **if** $s > 1$ **then**

5 Solve for $\omega^{(s)}$ as the solution of linear equation $L^{(s-1)} \omega^{(s)} = G_{\tau, j}^{(s-1)}$, and then construct

$$L^{(s)} \leftarrow \begin{bmatrix} L^{(s-1)} & \mathbf{0} \\ (\omega^{(s)})^\top & \sqrt{1 - (\omega^{(s)})^\top \omega^{(s)}} \end{bmatrix}$$

6 **end if**

7 Append the support set,

$$\tau^{(s)} \leftarrow \tau^{(s-1)} \cup j^{(s)} \quad (20)$$

which updates the support set corresponding to the signal estimate;

8 Update the signal estimate by solving the linear system,

$$\hat{\gamma}^{(s)} \leftarrow \text{Solve for } L^{(s)} (L^{(s)})^\top \gamma = \alpha_{\tau^{(s)}}^0 \quad \text{subject to } \operatorname{supp}\{\gamma\} = \tau^{(s)} \quad (21)$$

note that here the linear solver is performed over all x with support $\tau^{(s)}$;

9 Calculate

$$\alpha^{(s)} \leftarrow \alpha^0 - G_{\tau^{(s)}} \hat{\gamma}_{\tau^{(s)}}^{(s)} \quad (22)$$

to update the product term α ;

10 **end for**

Output: sparse code $\hat{\gamma}^{(S)}$.

which is sufficiently accurate for the online setting [30],

$$D_{:,j} \leftarrow \frac{1}{A_{jj}} (B_{:,j} - DA_{:,j} + D_{:,j} A_{jj}) \quad (27)$$

$$D_{:,j} \leftarrow D_{:,j} / \|D_{:,j}\|_2. \quad (28)$$

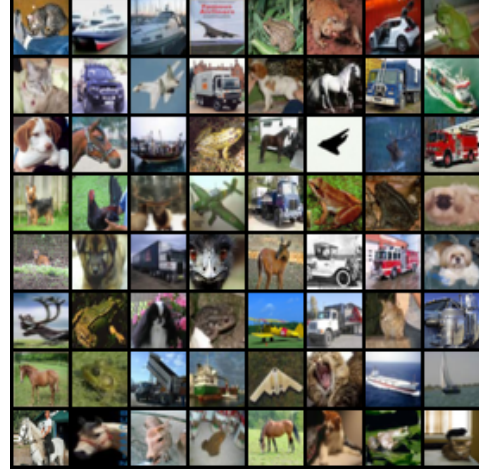


Figure 13. Target Images.

With sufficient number of training iterations and an accurate enough sparse coding stage, we expect the model training to converge. However, in practice this algorithm is slow when the number of dictionary atoms is large and does not yield necessarily superior performance compared to our implicit method, thus we do not adopt this method in the actual implementation but still we provide the implementation in the codebase for future potential improvements.

9. More Results from Training Experiments

Here we provide some additional results from our training experiments. Here in the following sections we majorly focus on comparing the VQ and DL family models to evaluate the performance of the compression bottleneck, hence models like VQ-VAE2 [41] that stacks two bottlenecks together are not relevant in comparing one unit of the bottleneck performance, also models like ViT-VQGAN [52] that use different encoder and decoder architectures while keeping the compression bottleneck intact are also not relevant for our comparisons. We still use the same hyperparameter setting for both of the models. In the main paper, with codebook/dictionary of size 512×16 and sparsity level 5 for the DL family models, the encoder and decoder architectures for both of the VQ and DL models are also the same as mentioned in the main paper, we also implemented the same PatchGAN discriminator architecture as suggested in [14, 22]. For the CIFAR10 dataset [29], we performed a 50,000/10,000 train-test split and trained with a batch size of 256 for 200 epochs, with additional 20 epochs when there's discriminator training, the results are as follows,

Table 2 summarizes the numeric evaluation results of the two models on CIFAR10 dataset,

We have also evaluated our models on the Flickr-Faces HQ (FFHQ) dataset [25], which contains 70,000 high qual-

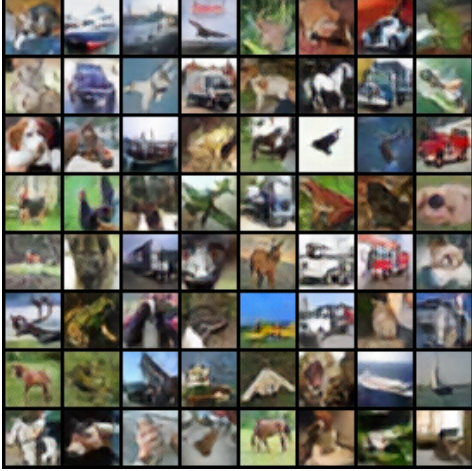


Figure 14. VQ-GAN Reconstructions.

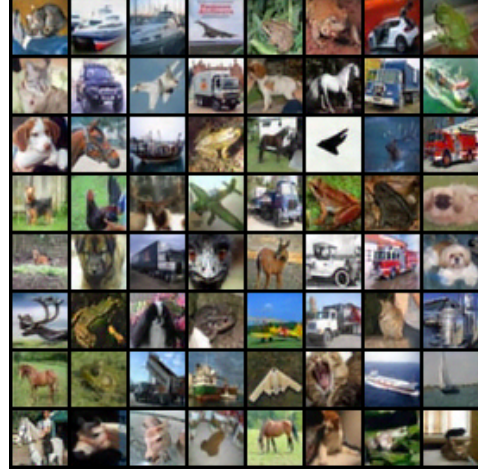


Figure 16. DL-GAN Reconstructions.

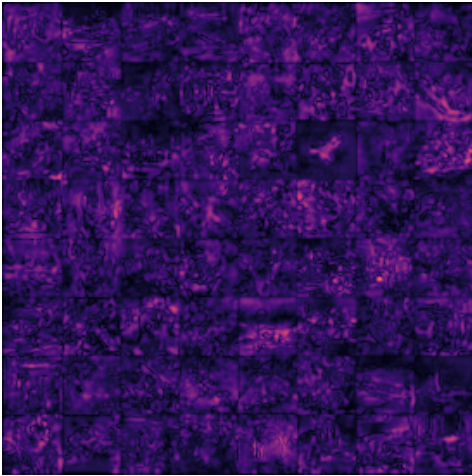


Figure 15. FLIP Heatmap of the VQ-GAN Reconstructions.

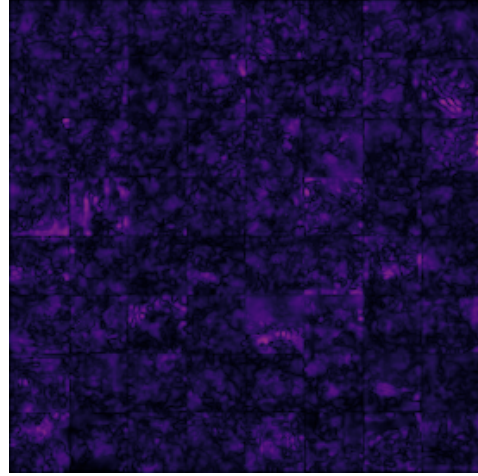


Figure 17. FLIP Heatmap of the DL-GAN Reconstructions.

Model	PSNR	LPIPS	FLIP
VQ-VAE	22.36	0.1629	0.05842
VQ-GAN	26.47	0.07492	0.05358
DL-VAE	28.81	0.02903	0.05181
DL-GAN	30.01	0.01745	0.04792

Table 2. Reconstruction evaluations on the CIFAR10 dataset.

Model	PSNR	LPIPS	FLIP
VQ-VAE	23.45	0.1576	0.09929
VQ-GAN	25.67	0.1029	0.08244
DL-VAE	30.80	0.03749	0.07783
DL-GAN	32.93	0.02507	0.06427

Table 3. Reconstruction evaluations on the CIFAR10 dataset.

ity 1024×1024 RGB images of human faces. For the training setup, we performed a 60,000/10,000 train-test split and downsampled the images to 512×512 to fit in our GPU memory. We trained both VQ and DL family models on the dataset with a batch size of 8 for 20 epochs, with additional 5 epochs for discriminator training. The results are shown in the figures below,

Table 3 summarizes the numeric evaluation results of the two models on FFHQ dataset

From the above training experiment results, we can see the DL family models demonstrate superior performance compared to VQ family models by a comfortable margin.

10. Impact of Codebook/Dictionary Sizes

To analyze the impact of codebook/dictionary sizes on the models, we evaluated both VQ and DL family models on the CIFAR10 dataset [29] with varying codebook/dictionary



Figure 18. Target Images.



Figure 19. VQ-GAN Reconstructions.

Size	VQ-VAE	VQ-GAN	DL-VAE	DL-GAN
64	22.53	23.69	26.79	27.85
256	23.59	25.74	28.03	29.91
512	22.36	24.93	28.95	30.04

Table 4. Reconstruction evaluations on the CIFAR10 dataset on varying codebook/dictionary sizes.

sizes for 100 epochs, with additional 20 epochs for discriminator training, the resulting reconstruction PSNRs are summarized in the table 4. Note that for all the DL family models experiments we use a sparsity level of 4.

11. Ablation Studies on Sparsity Levels

We perform ablation studies with respect to the sparsity level of the Dictionary Learning Compression Bottleneck, we evaluated the DL-VAE model on the CIFAR10 dataset [29] with varying sparsity levels with fixed dictionary size as 512 for 100 epochs, the resulting reconstruction evaluations are summarized in the table 5.

From the above evaluations we can see that the DL-VAE model gains more representation power as the sparsity level goes up, but loses dictionary perplexity at the mean time, we contend that including more dictionary atoms for each

Sparsity	PSNR	Perplexity
2	25.63	504
4	28.95	507
5	29.33	498
8	31.32	455
10	31.96	428

Table 5. Reconstruction evaluations on the CIFAR10 dataset on varying sparsity levels.

latent feature vector gives the dictionary atoms a tendency to become more similar to each other.

12. Downstream Generation

In the following sections we evaluate our model with downstream generation tasks such as super-resolution, inpainting, and text-to-image generation with Stable Diffusion [42]. Note that the purpose of this section is not trying to prove our model beats the state-of-the-art generative models, but rather to show the versatile generation power gained by simply restructuring the latent space, we’ll focus on the VQ-VAE and DL-VAE model training for the following sections to compare their compression bottleneck performance, and we purposefully disallow the discriminator training so that the additional generation power from the

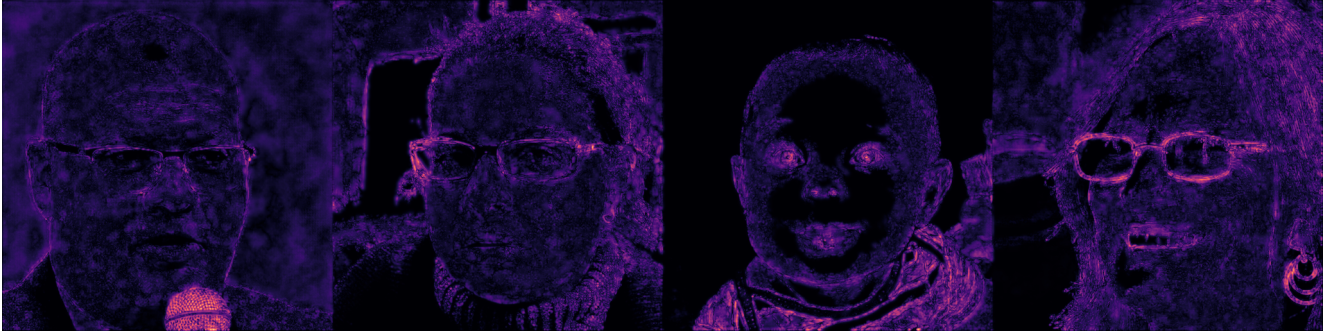


Figure 20. FLIP Heatmap of the VQ-GAN Reconstructions.



Figure 21. DL-GAN Reconstructions.

discriminator will not interfere our evaluations on the compression bottleneck performance.

12.1. Single Image Super Resolution Experiments

For the single image super resolution experiments, we evaluated our models on the Oxford Flowers dataset [33] by first downsampling the images to 64×64 dimension and then upscaling to 256×256 dimension via bicubic degradation [26] as the input data, with the original images as the target super resolved images. We trained the VQ-VAE and DL-VAE models on the same dataset with a batch size of 8 for 2,000 epochs. For evaluation we also use the Fréchet Inception Score (FID, the lower the better) to measure the generation quality [19]. The results are as follows,

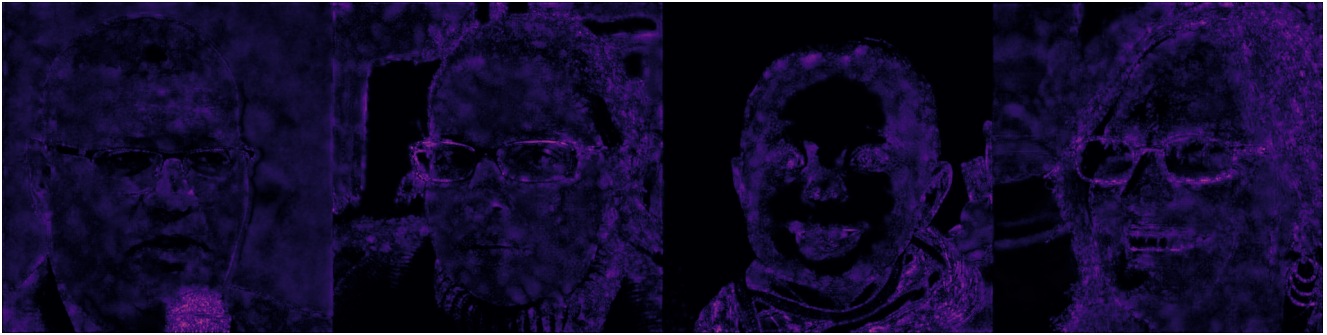


Figure 22. FLIP Heatmap of the DL-GAN Reconstructions.



Figure 23. Bicubic Downsampled Low Resolution Inputs.

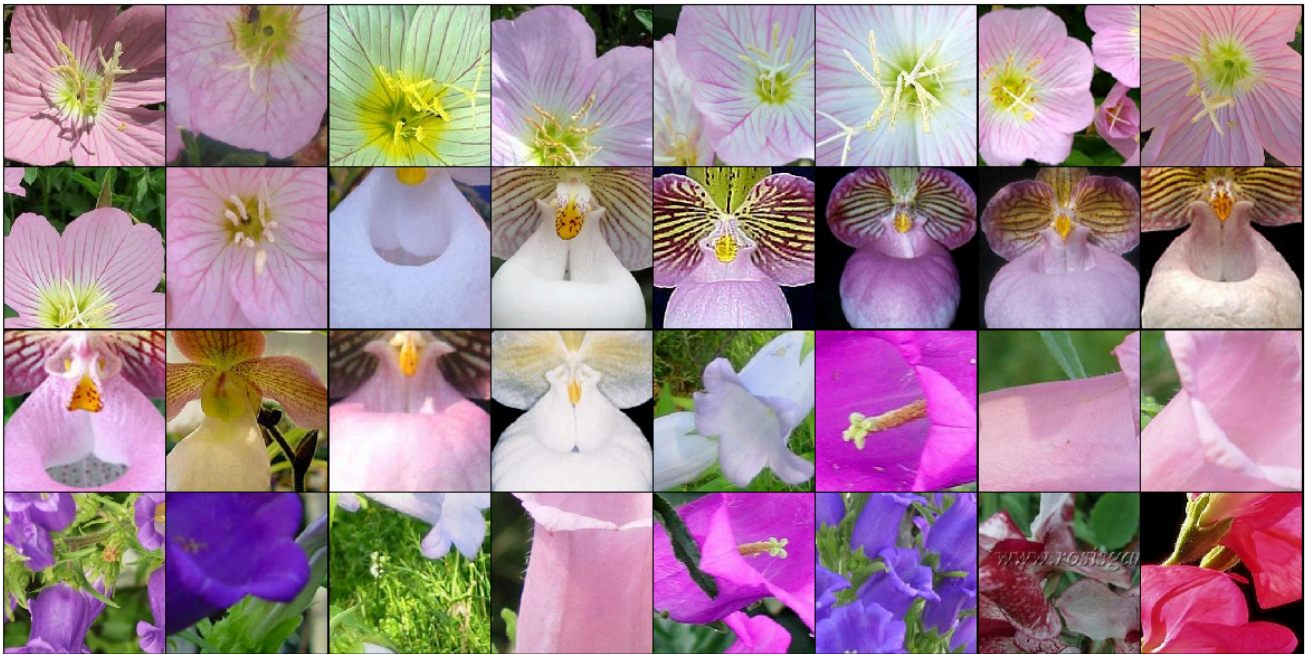


Figure 24. Target Images for Single Image Super Resolution.

Model	PSNR	FLIP	FID
VQ-VAE	28.78	0.1219	33.89
DL-VAE	29.23	0.08767	23.31

Table 6. Single image super resolution on Oxford Flowers dataset.

Table 6 is a brief summary of the quantitative evaluations of the super resolution experiments for both models.

From the results we can see the DL-VAE model provides more representation power as compared to VQ-VAE in the latent space while all the other model architectural components (encoder, decoder networks) remain the same.

12.2. Inpainting

To evaluate the latent representation power of the compression bottleneck in terms of inpainting, we trained the VQ-VAE and DL-VAE models on the Oxford Flowers dataset for the same setting as before for 1,000 epochs. For the input images, we apply a square bitmask that’s 0.25 fraction of the image dimension in the center of the images to mask out the pixels (set the pixel values to 0). The results are as follows, we have also provided the reconstructed latent space top singular component visualizations to see how the masking affects the latent space,

The numerical evaluation results of the inpainting experiments are summarized in Table 7.

We can observe interestingly although the DL-GAN still demonstrates better performance overall but is also sensitive to the added noise from masking as the VQ-VAE.

12.3. Restructuring the Latent Space of the Stable Diffusion Models

We have also applied the VQ-VAE and DL-VAE models’ compression bottlenecks to the latent space of the Stable Diffusion models [42] for simple text-to-image generation tasks, during these experiments we fix the encoder and decoder network of the pretrained stable diffusion network along with the weights of the diffusion U-Net [21, 42] and finetune the Vector Quantization bottleneck for a moderate amount of training steps (100), note that here a big advantage of our Dictionary Learning formulation is that once the dictionary is learned and fixed, since the sparse coding stage is deterministic, we do not need any additional finetuning to

Model	PSNR	FLIP	FID
VQ-VAE	28.78	0.1301	72.19
DL-VAE	30.08	0.1098	59.48

Table 7. Inpainting evaluations on the Oxford Flowers dataset.

Structure	PSNR	FLIP	FID
Vector Quantization	14.70	0.1301	63.90
Dictionary Learning	58.06	0.006690	0.01061

Table 8. Evaluations on the Latent Space Structuring Strategies for Stable Diffusion.

apply the Dictionary Learning bottleneck to the Stable Diffusion model. Some of the results from our experiments are shown in the images below,

The numerical evaluation results of the inpainting experiments are summarized in Table 8.

From the experiments we can clearly see the quantization artifacts from the Vector Quantization bottleneck, the Dictionary Learning Bottleneck, on the other hand, reconstructs the latent space with high fidelity.



Figure 25. Super Resolved Images from VQ-VAE

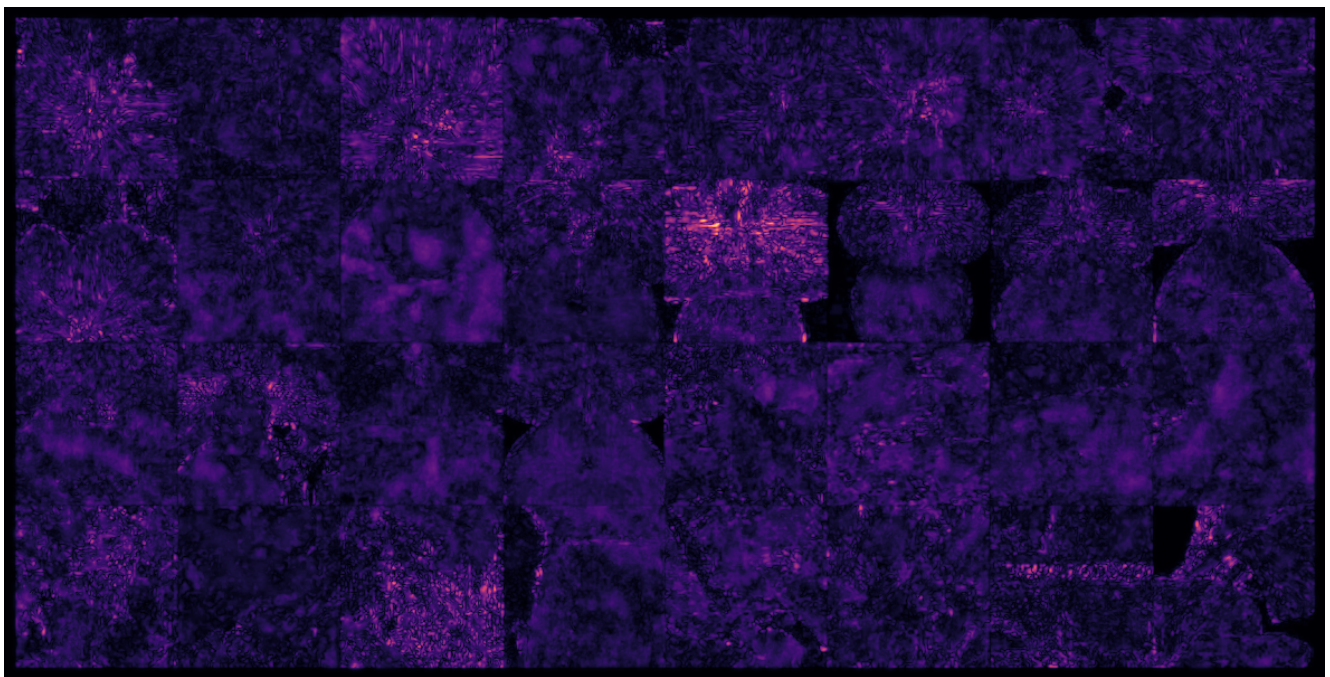


Figure 26. Flip Heatmap Evaluations for the VQ-VAE Super Resolution.



Figure 27. Super Resolved Images from DL-VAE

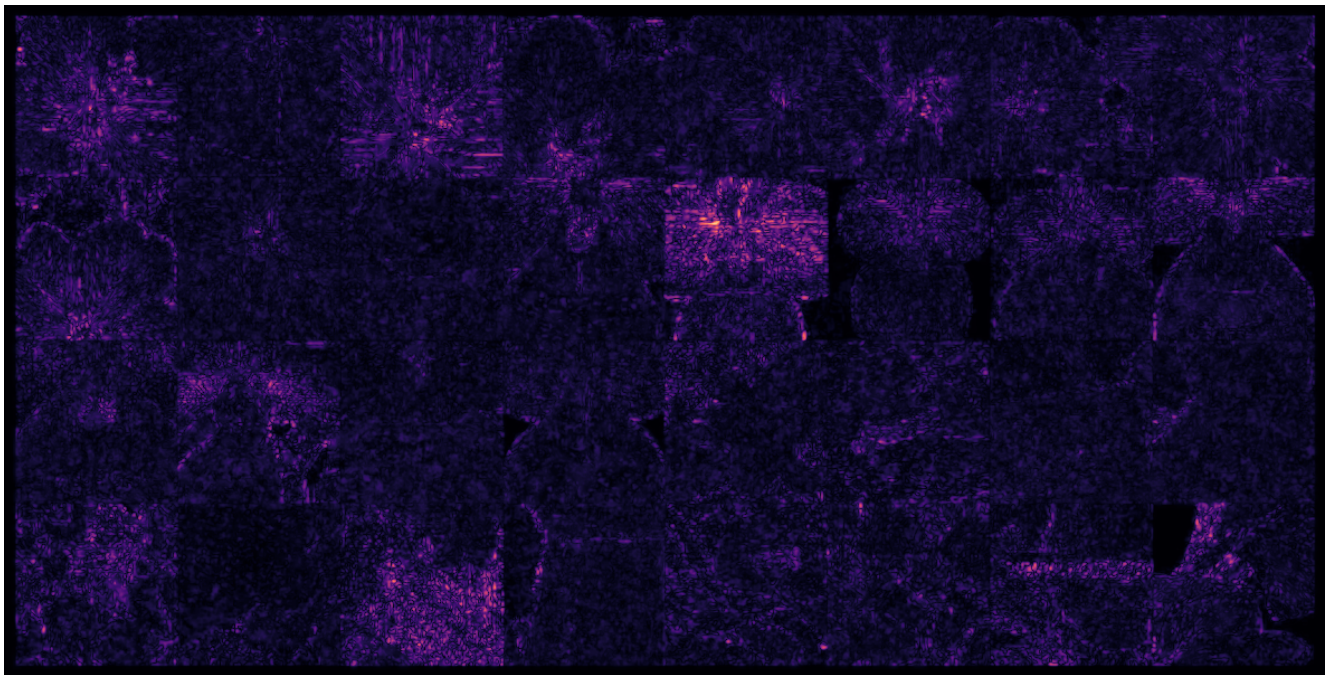


Figure 28. Flip Heatmap Evaluations for the DL-VAE Super Resolution.



Figure 29. Original Input Images for Inpainting.



Figure 30. Masked Inputs.



Figure 31. VQ-VAE Inpainting Results.

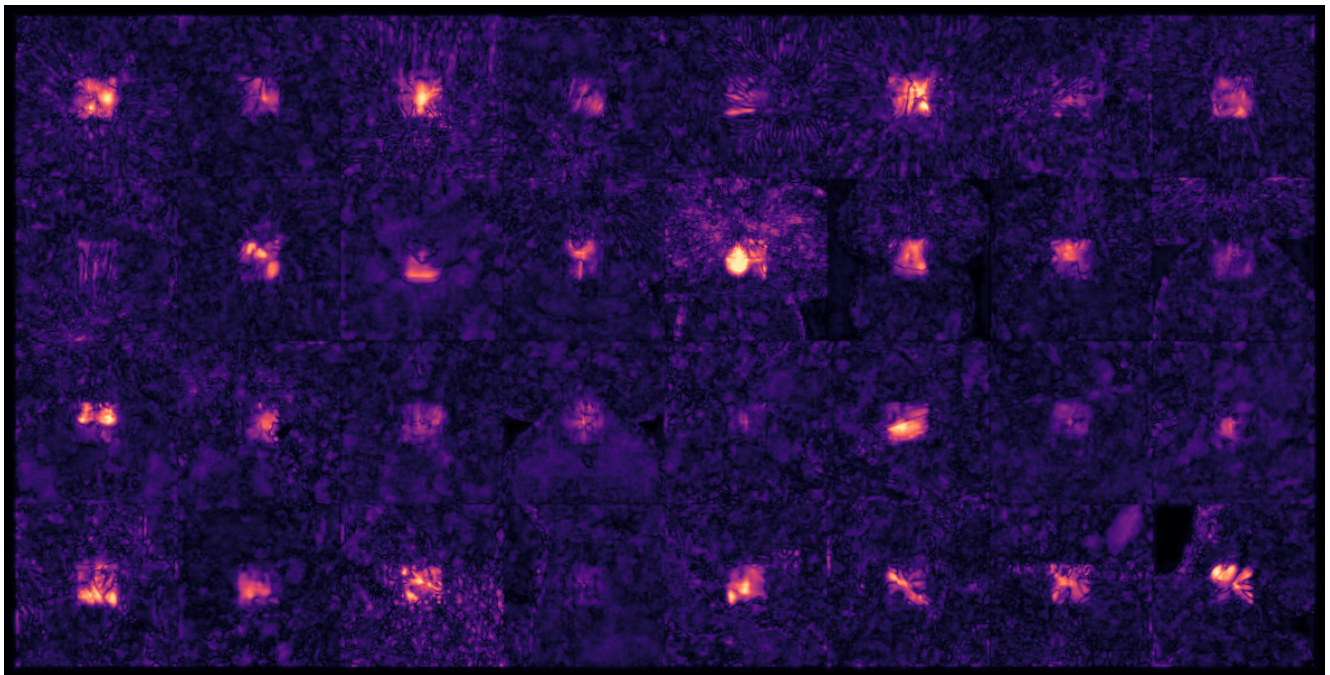


Figure 32. FLIP Heatmap Evaluations for VQ-VAE Inpainting.

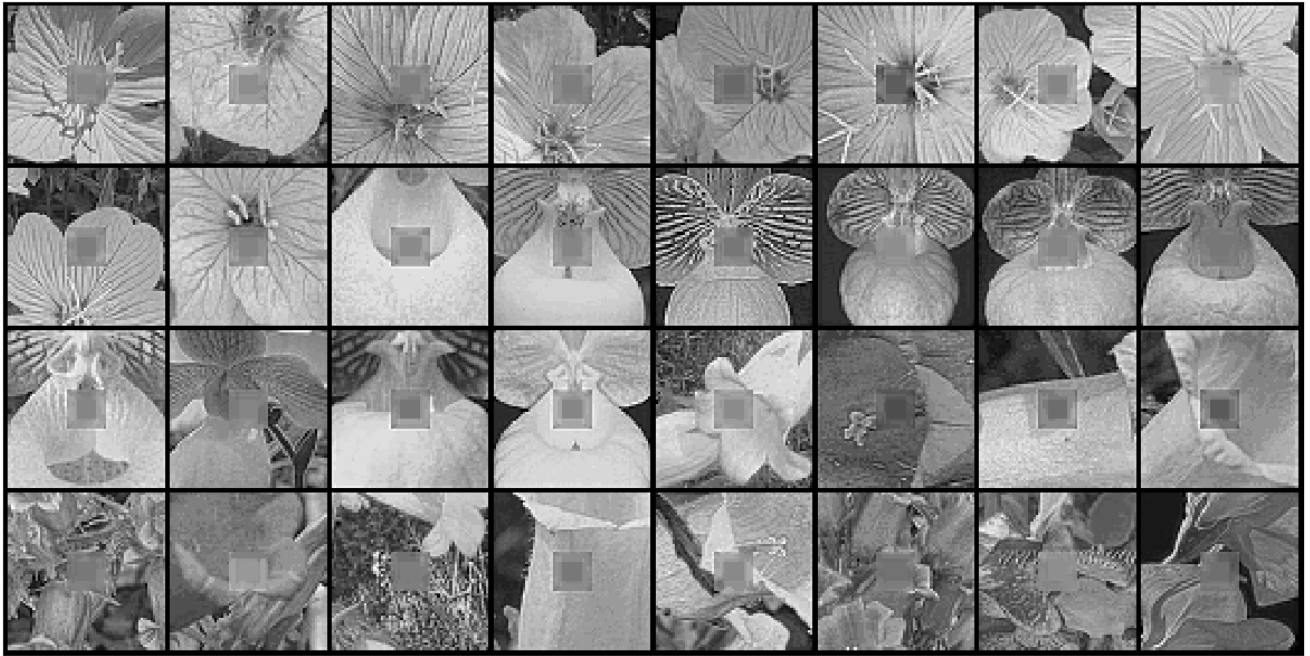


Figure 33. Top singular component of the VQ reconstructed latent space.



Figure 34. DL-VAE Inpainting Results.

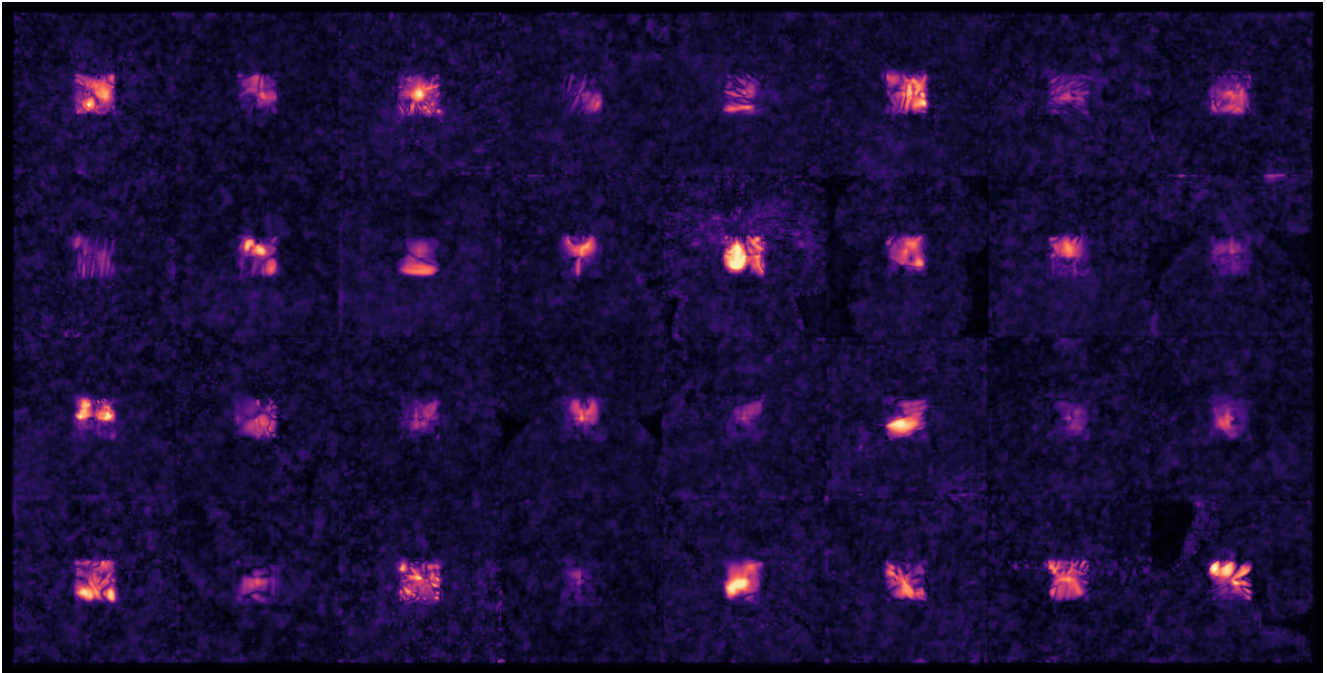


Figure 35. FLIP Heatmap Evaluations for DL-VAE Inpainting.

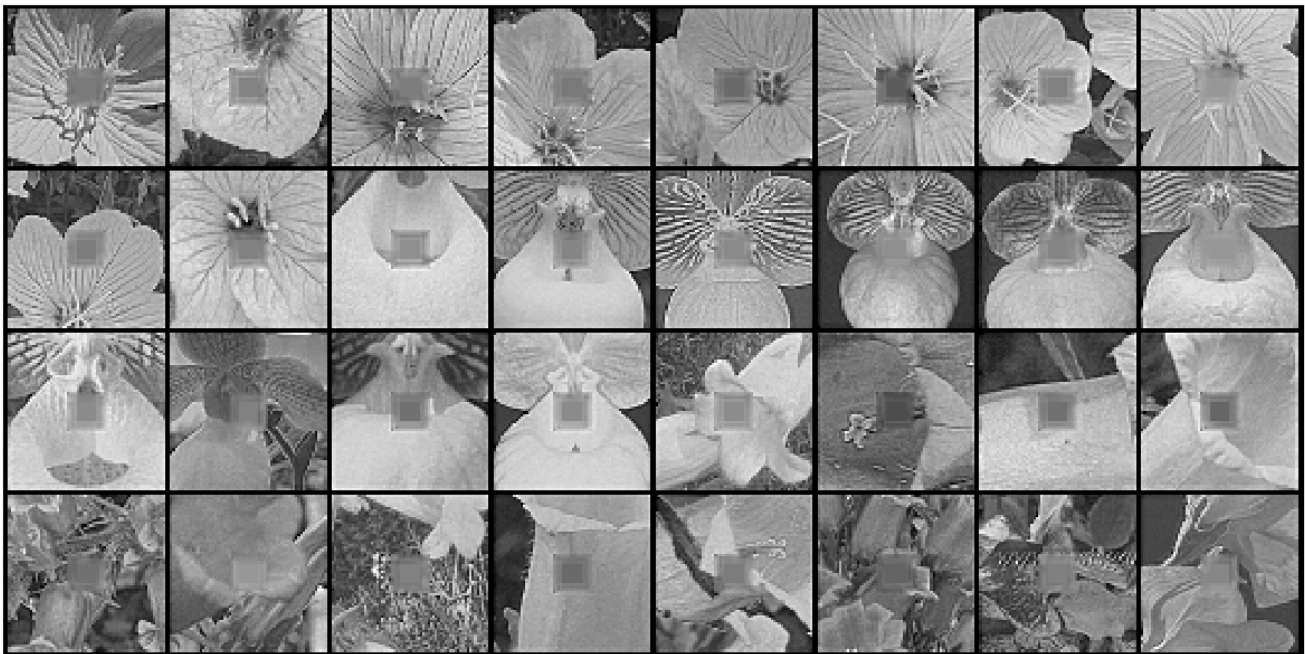


Figure 36. Top singular component of the DL reconstructed latent space.

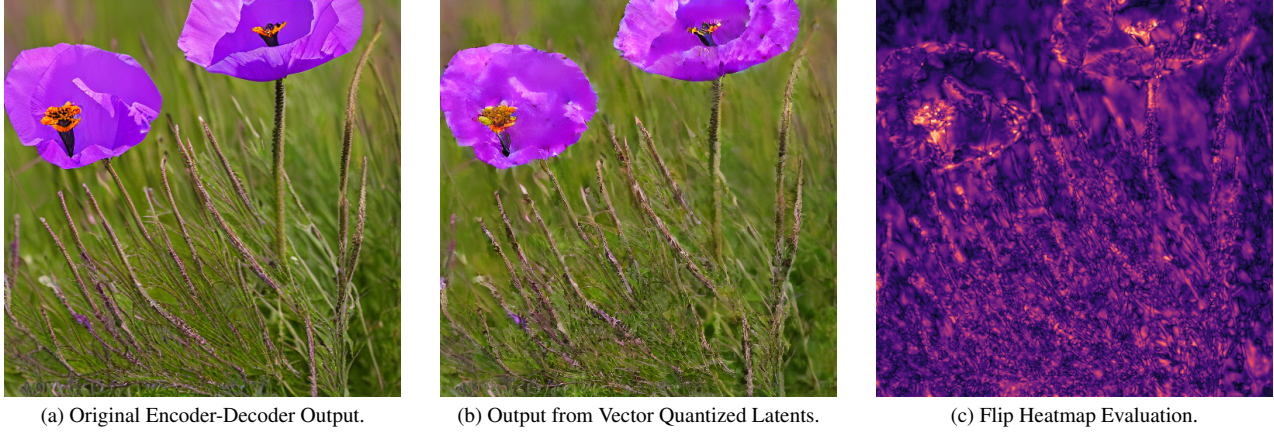


Figure 37. Comparison between the latent space attained from the original encoder-decoder of Stable Diffusion and the Stable Diffusion with vector quantized latent space given the Prompt: “purple californian poppy” (the flower is yellow).



Figure 38. Comparison between the latent space attained from the original encoder-decoder of Stable Diffusion and the Stable Diffusion with dictionary learned latent space given the Prompt: “purple californian poppy” (the flower is yellow).

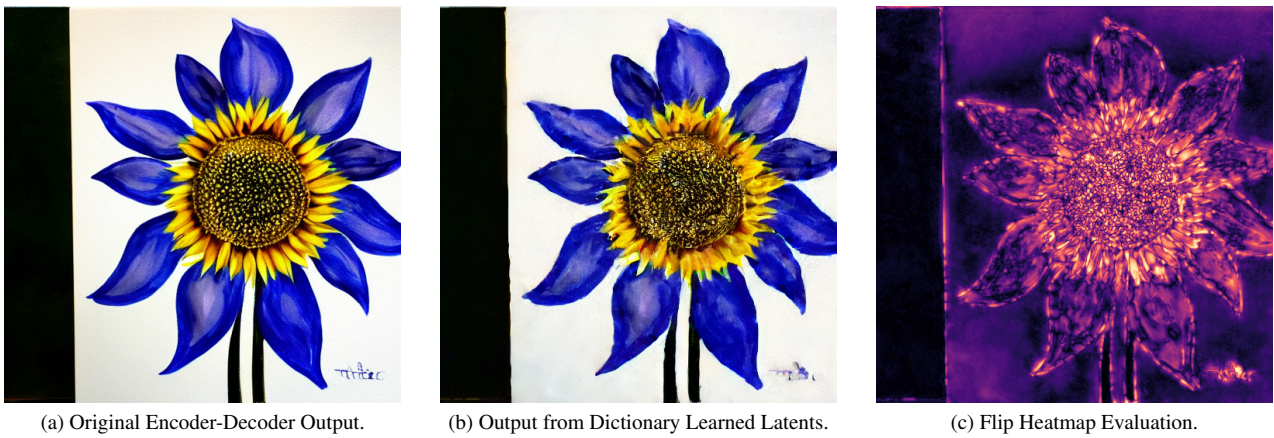


Figure 39. Comparison between the latent space attained from the original encoder-decoder of Stable Diffusion and the Stable Diffusion with vector quantized latent space given the Prompt: “blue sunflower” (the flower is yellow).

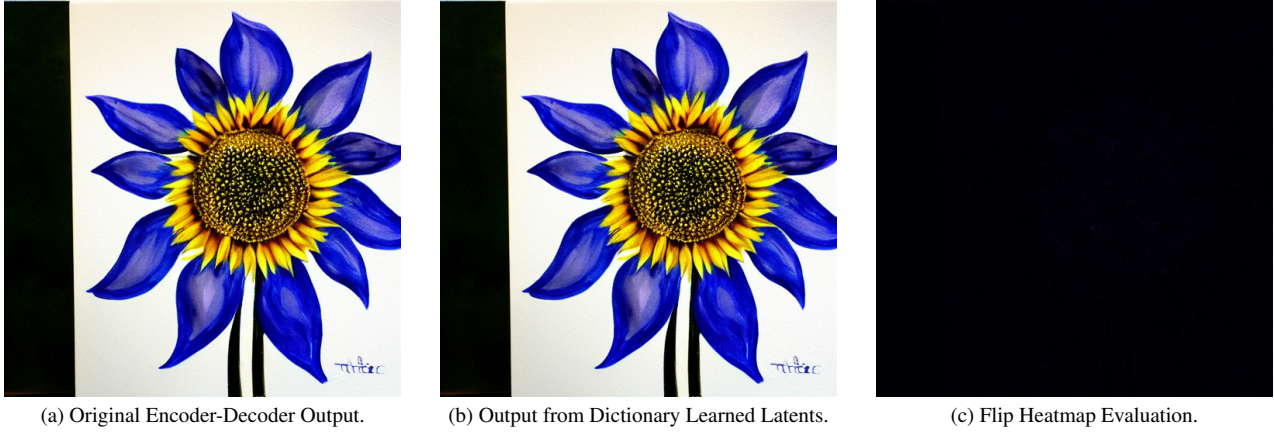


Figure 40. Comparison between the latent space attained from the original encoder-decoder of Stable Diffusion and the Stable Diffusion with dictionary learned latent space given the Prompt: “blue sunflower” (the flower is yellow).



Figure 41. Comparison between the latent space attained from the original encoder-decoder of Stable Diffusion and the Stable Diffusion with vector quantized latent space given the Prompt: “astronaut corgi on the moon”.

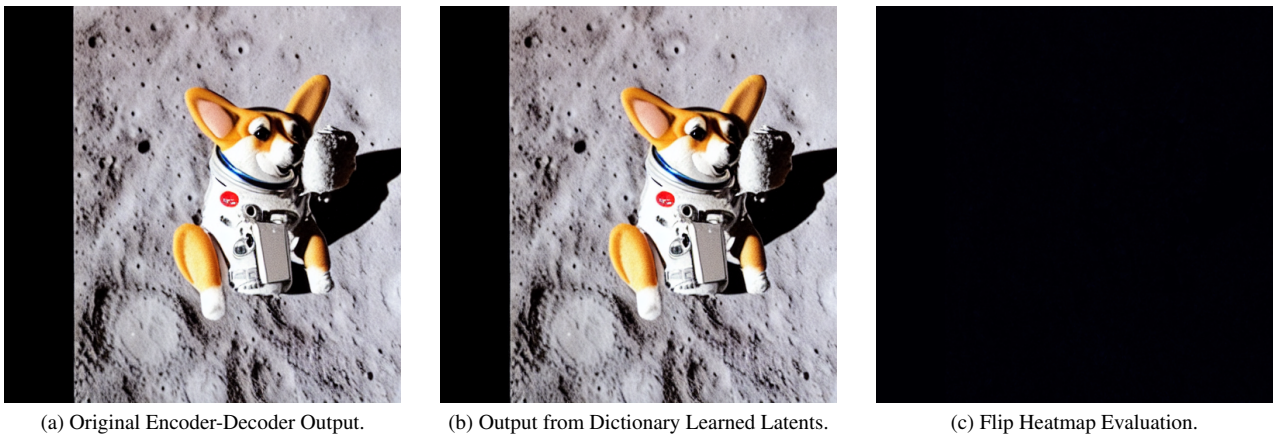


Figure 42. Comparison between the latent space attained from the original encoder-decoder of Stable Diffusion and the Stable Diffusion with dictionary learned latent space given the Prompt: “astronaut corgi on the moon”.